

# Quantum Monte Carlo at the Graphene Quantum Hall Edge

Zhenjiu Wang,<sup>1,\*</sup> David J. Luitz,<sup>2,1</sup> and Inti Sodemann Villadiego<sup>3,1,†</sup>

<sup>1</sup>*Max-Planck-Institut für Physik komplexer Systeme, Dresden 01187, Germany*

<sup>2</sup>*Physikalisches Institut, University of Bonn, Nussallee 12, 53115 Bonn, Germany*

<sup>3</sup>*Institut für Theoretische Physik, Universität Leipzig, D-04103, Leipzig, Germany*

We study a continuum model of the interface of graphene and vacuum in the quantum hall regime via sign-problem-free quantum Monte Carlo, allowing us to investigate the interplay of topology and strong interactions in a graphene quantum Hall edge for large system sizes. We focus on the topological phase transition from the spin polarized state with symmetry protected gapless helical edges to the fully charge gapped canted-antiferromagnet state with spontaneous symmetry breaking, driven by the Zeeman energy. Our large system size simulations allow us to detail the behaviour of various quantities across this transition that are amenable to be probed experimentally, such as the spatially and energy-resolved local density of states and the local compressibility. We find peculiar kinks in the branches of the edge dispersion, and also an unexpected large charge susceptibility in the bulk of the canted-antiferromagnet associated with its Goldstone mode.

*Introduction.* The quantum Hall regime in graphene-based systems has emerged as a fantastic arena for investigating correlated and topological states of electrons. Progress on ingenious experimental techniques, such as compressibility measurements [1–4], non-local magnon transmission [5–10], scanning-tunneling microscopy, and others [11–13], have allowed to paint a remarkably rich picture on the interplay of symmetry breaking and topology in these systems. In particular at charge neutrality an interaction driven integer quantum Hall ferromagnet is seen in experiments [14–17], which can be driven into a spin polarized state via in-plane Zeemann coupling [18] and with an STO substrate [19]. The landscape of possible interaction driven states at neutrality, which likely depends on the substrate, still remains to be fully understood. While some experiments have been consistently interpreted by viewing the state as canted antiferromagnet [10, 13, 18, 20, 21], recent STM experiments have reported a prevalence of Kekule-type valence bond solid states [22–24].

In this letter we investigate via sign-problem-free Quantum Monte Carlo (QMC) the proposed topological phase transition at neutrality from a canted antiferromagnet with gapped edges into a quantum spin Hall state with topologically protected counter-propagating modes [25]. To this date theoretical studies of this edge phase transition have been restricted to mean field and analytical field theoretical studies [26–30], but there has not been an unbiased numerical study of this transition.

We have found several noteworthy features. First, the edge displays a clear insulator to helical metal phase transition by increasing the Zeeman field, as expected, but in contrast to Hartree-Fock studies[29], the charge gap at the edge opens up concomitantly with the spontaneous symmetry breaking transition in the bulk from spin po-

larized to canted-antiferromagnetic state. This reflects the Mermin-Wagner-type destruction of long-range order of the XY spin edge texture of Ref. 29 from quantum fluctuations as discussed in field theoretical models [26, 31]. Nevertheless, we observe clear kinks in the quasiparticle dispersion of the helical edge of the topological spin polarized state as a function of the distance to the edge, that are visible even at the metal-insulator critical point, which closely resemble the kinks reported in the Hartree-Forck study of Knothe and Jolicoeur [29]. In an effort to guide future STM studies, we show how these kinks would appear in the spatially resolved local density of states. We have also found a substantially large bulk local charge susceptibility in the canted-antiferromagnetic state in contrast with the spin polarized state. This enhancement of the charge susceptibility can be suppressed by adding explicit symmetry breaking fields that gap the goldstone modes of antiferromagnet. This prediction could help guide the distinction of these correlated states in future measurements of local compressibility.

*Model.* We are interested in the half-filled zeroth Landau level (ZLL) of graphene. We therefore project the Hilbert space onto the 4 component spin/valley ZLL, such that there are  $4N_\phi$  single particle states in a torus pierced by  $N_\phi$  flux quanta. The fermion annihilation operators in real space are projected as:  $\hat{\psi}_a(\mathbf{x}) = \sum_{n_k=1}^{N_\phi} \phi_{n_k}(\mathbf{x}) \hat{c}_{a,n_k}$  ( $a = 1, 2, 3, 4$ ). Here  $\hat{c}_{a,n_k}$  is the canonical fermion operator that annihilates a fermion at momentum  $k = 2\pi n_k/L_y$  and flavor  $a$ , and  $\phi_{n_k}(\mathbf{x})$  is the  $n_k$ th single particle ZLL wave function in Landau gauge ( $\mathbf{A}(\mathbf{x}) = B(0, x)$ ). The model Hamiltonian reads:

$$\hat{H} = \hat{H}_{\text{Bulk}} + \hat{H}_{\text{Edge}}, \quad (1)$$

where the bulk Hamiltonian is the model introduced by Kharitonov [32], which has been successfully exploited to investigate the quantum hall regime of graphene[33]. This model includes an  $SU(4)$  invariant long range Coulomb interaction, a short range anisotropic interac-

\* zhwang@pks.mpg.de

† sodemann@pks.mpg.de

tion, as well as the Zeeman coupling:

$$\hat{H}_{\text{Bulk}} = \hat{H}_{\text{Ani}} + \hat{H}_{\text{Coul}} + \hat{H}_{\text{Zeeman}}, \quad (2)$$

with

$$\hat{H}_{\text{Coul}} = \frac{1}{2} \int_V \int_V d\mathbf{x} d^2\mathbf{x}' \delta\hat{\rho}(\mathbf{x}) V(\mathbf{x} - \mathbf{x}') \delta\hat{\rho}(\mathbf{x}'), \quad (3)$$

Here  $V(\mathbf{x} - \mathbf{x}') \equiv e^2/\epsilon|\mathbf{x} - \mathbf{x}'| - e^2/\epsilon\sqrt{|\mathbf{x} - \mathbf{x}'|^2 + d^2}$ , with  $d/2$  the distance to a screening gate, and  $\delta\hat{\rho}(\mathbf{x}) = \hat{\psi}^\dagger(\mathbf{x})\hat{\psi}(\mathbf{x}) - n_0$ , the density deviation away from half-filling,  $n_0 = 1/(\pi l_B^2)$ , ensuring particle-hole symmetry. The interaction anisotropy term read as:

$$\hat{H}_{\text{Ani}} = \frac{1}{2} \int_V d^2\mathbf{x} [g_z \hat{\tau}_z^2(\mathbf{x}) + g_\perp (\hat{\tau}_x^2(\mathbf{x}) + \hat{\tau}_y^2(\mathbf{x}))], \quad (4)$$

where  $\hat{\tau}_i(\mathbf{x}) = \hat{\psi}^\dagger(\mathbf{x})\tau_i\hat{\psi}(\mathbf{x})$ , where  $\tau_i$  are the Pauli matrices in valley space. The term  $\hat{H}_{\text{Zeeman}} = h \int_V d^2\mathbf{x} \hat{\psi}^\dagger(\mathbf{x})\sigma^z\hat{\psi}(\mathbf{x})$  is the standard Zeeman coupling (with g-factor  $g = 2$ ) controlled by magnitude of the total magnetic field including its perpendicular and in-plane components. Increasing Zeeman coupling  $h$  favors the spin polarized state, which is achieved once it exceeds the critical value  $4\pi l_B^2 h_c/g_\perp = 2/\pi$ .

The phase diagram of the bulk state is well understood [32]: a Kekule-valence-bond phase, an anti-ferromagnetic state (AFM), a charge-density wave state, as well as a ferromagnetic (FM) state as depicted in the inset of Fig. 1. Throughout this study we will focus on the case of  $g_\perp < 0$ , choosing  $g_z = -2g_\perp$  that allows to probe the FM to AFM transition. Even though the charge gap remains finite across this transition, there is a change of the topology of the bulk state accompanied by an edge transition, characterised by the change of the spin chern number,  $C \equiv C_\uparrow - C_\downarrow$  [34], which is closely related to  $Z_2$  time reversal invariant insulators [35, 36], albeit without time reversal symmetry. Here the FM state is the topologically non-trivial state with gapless helical edge modes protected by separate particle number conservation of spin up and down particles. This symmetry is spontaneously broken in the CAF state, gapping out as a result the edge states [25, 27].

In order to study the edge physics, we gap half of the torus by a Kekule mass term:

$$\hat{H}_{\text{Edge}} \equiv \Delta \int_V d^2\mathbf{x} \hat{\psi}^\dagger(x, y) \tau^x \otimes \sigma^0 \hat{\psi}(x, y) s(x), \quad (5)$$

where  $s(x)$  is a smooth function that depends only on the  $x$  direction which we take to be :

$$s(x) \equiv \sum_n g(x + L_x) \quad n \in Z$$

$$g(x) \equiv \frac{1}{2} (\tanh[(x - \frac{1}{4}L_x)/\xi] + \tanh[(x + \frac{1}{4}L_x)/\xi]) + 1. \quad (6)$$

Here  $s(x)$  is nearly 0 for  $0 < x < L_x/4$  and  $3L_x/4 < x < L_x$ , and changing over a typical length  $\xi$ . The region where  $s(x) \approx 1$  can be interpreted as a trivial vacuum, with zero spin and charge Chern numbers, and therefore serves as toy model to generically capture the physical interface of Graphene with vacuum. Moreover, as argued in Ref. 27 and Ref. [29], the edge separating such vacuum regions (with  $s(x) \approx 1$ ) from the system of interest (with  $s(x) \approx 0$ ) can be viewed as a continuum approximation of the physical armchair boundaries of Graphene.

The applicability of QMC simulation without sign problem for these terms has been previously discussed in Refs. [37, 38], and we summarize it in Supplemental material A. We use the finite temperature auxiliary field method [39–41] of the algorithms for lattice fermions (ALF)-library [42].

*Numerical results.* We take the following values for the parameters that have been estimated from experiments [10, 20, 21, 43–47]  $h = \mu_B \sqrt{(B_\perp^2 + B_\parallel^2)}$ ,  $g_\perp/(2\pi l_B^2) = g_z/(4\pi l_B^2) = 10h$ , and  $e^2/(4\pi\epsilon l_B) \approx 217.63\sqrt{B_\perp}$  where we take the dielectric constant  $\epsilon = 4.5$ , relevant for Graphene suspended in vacuum and dressed by RPA corrections [48].

As a first non-trivial benchmark, we will compare the bulk charge gap from our QMC calculations and that of Hartree-Fock theory (for details of HF calculation see supplementary section B):

$$\Delta_{sp} = \left\{ \left[ \frac{1}{4\pi} (\tilde{\mu}_c + \mu_z - 2|\mu_\perp|) \cos\theta + h \right]^2 + \left[ \frac{1}{4\pi} (\tilde{\mu}_c + \mu_z + 2|\mu_\perp|) \sin\theta \right]^2 \right\}^{1/2}, \quad (7)$$

where  $\mu_z \equiv g_z/(2\pi l_B^2)$ ,  $\mu_\perp \equiv g_\perp/(2\pi l_B^2)$  and  $\tilde{\mu}_c \equiv \frac{1}{N_\phi} \sum_{\mathbf{q}} f(\mathbf{q})f(-\mathbf{q})V_0(\mathbf{q})(e^2)/(\epsilon l_B) = 0.8328(e^2)/(\epsilon l_B)$ . On the other hand,  $\Delta_{sp}$  from QMC can be obtained from the asymptotic decay of the Green's function along the imaginary axis as follows:

$$\frac{1}{V} \int_V d^2\mathbf{x} \sum_a \langle \hat{\psi}_a^\dagger(x, y, \tau) \hat{\psi}_a(x, y, 0) \rangle \propto e^{-\tau \Delta_{sp}(N_\phi)}. \quad (8)$$

The calculation is performed for  $N_\phi = 16, 24, 32, 40$  and 48, with  $\beta g_\perp/(4\pi l_B^2) = N_\phi/2$  and  $4\pi l_B^2 \Delta_\tau/g_\perp = 4/N_\phi$  (see Ref. [38] for details). We observed very robust system size dependence of  $\Delta_{sp}(N_\phi)$ , allowing reliable extrapolation to the thermodynamic limit. The  $B_\perp$  dependence of gap in the absence of  $B_\parallel$  are plotted in Fig. 1 as purple dots, where we see an excellent agreement with HF estimates. We have also performed benchmark calculations of the order parameters that allowed us to verify that the bulk phase transition of the CAF to FM indeed occurs at the critical value of  $4\pi l_B^2 h_c/g_\perp = 2/\pi$ .

After having benchmarked the bulk behavior, we move to the main focus of our work, which is the study of the edge transitions. We pick up  $B_\perp = 4.7358T$  and will

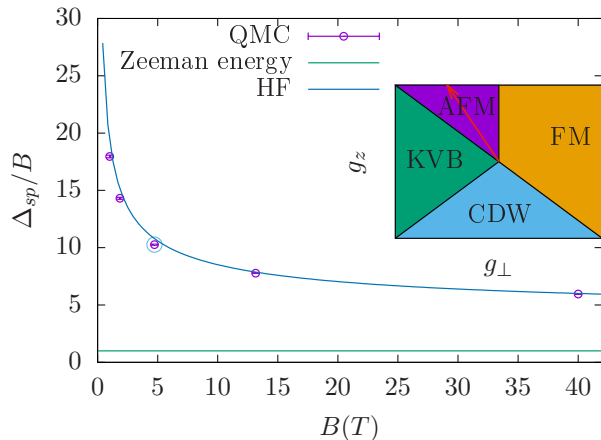


FIG. 1.  $B_{\perp}$  dependence of bulk single particle gap based on QMC simulation and HF theory. Blue circle corresponds to the point ( $B_{\perp} = 4.7358T$ ) that we use for studying edge states. Blue line is the gap from HF approximation based on Eq. 24. Inset: phase diagram of graphene quantum Hall states at neutrality.

work in the energy unite where  $g_{\perp}/(4\pi l_B^2) = 1$ . We will illustrate the behavior for three characteristic values of Zeeman couplings  $h_c = 1.2(\text{FM})$ ,  $2/\pi(\text{critical point})$ , and  $0.2(\text{CAF})$ . The Kekule potential energy in the ‘vacuum’ and the typical length are chosen as  $\Delta = 6$  and  $\xi = 0.5$ . One of the key physical observables that describes the edge is the single particle local density of states:

$$A_{\psi}(x, \omega) = \frac{1}{Z} \sum_{i,j,a} |\langle i | \hat{\psi}_a(x, y) | j \rangle|^2 (e^{-\beta E_i} + e^{-\beta E_j}) \times \delta(E_i - E_j - \omega), \quad (9)$$

which is  $y$  independent.  $E_i$  is the  $i$ th eigenvalue of Hamiltonian. This quantity is extracted from the imaginary time correlation function:

$$\sum_a \langle \hat{\psi}_a^{\dagger}(x, y, \tau) \hat{\psi}_a(x, y, 0) \rangle \quad (10)$$

via the stochastic maximum entropy method [42, 49]. For the simulation of edge states, we focus on the system size of  $N_{\phi} = 48$ . An inverse temperature of  $\beta = 24$  is found to be sufficient to converge to the ground state, and the Trotter step is taken as  $\Delta_{\tau} = 0.2$ .

The presence of the topologically protected helical edge states can be detected by measuring the LDOS near the edge. At  $h = 1.2$ ,  $A_{\psi}(x, \omega)$  is characterised by linearly dispersing edge states around the boundary between FM bulk and Kekule vacuum at  $|x|/L_x \approx 0.25(0.75)$ , as shown in Fig. 2.(a). Remarkably, as we see in Fig. 2, clear kinks in the spatial dependence of the quasi-particle dispersion appear as one moves from the spin polarized bulk towards the trivial edge. Such features are absent in the simplified mean field treatment [27], but similar features

were found in the more systematic Hartree-Fock study of Ref. [29] Similar behavior exists at the FM-CAF critical point  $h_c = 2/\pi$ , even though the quasiparticle peaks are much broader in this case as seen in panels (d,e) of Fig. 2. On the other hand, we have found that at the critical point the electron quasiparticle gap at the edge vanishes in the thermodynamic limit, as further discussed in the Supplementary section C. This contrasts with the Hartree-Fock analysis of Ref. [29], but is consistent with Mermin-Wagner absence of long-range order for the XY spin projection for this helical Luttinger liquid as discussed in [26, 31]. Finally, at  $h = 0.2$ ,  $A_{\psi}(x, \omega)$  shows clearly gaped behavior at the edge due to the spontaneously broken  $\sigma_z$  conservation in the bulk, and also no strong kink-like features are seen in the edge quasiparticle spectrum. Another interesting finding is that the broadening of quasi-particle peaks originates primarily from the long range Coulomb interaction, and not from the short distance valley dependent interactions. We illustrate this in detail in the Supplementary Section D, where we show the sharp quasiparticle peaks that would appear in a model without the long range part of the Coulomb interactions.

We also determined the local charge susceptibility:

$$\chi_{\text{charge}}(x) = \int_0^{\beta} dt \langle \hat{\psi}^{\dagger}(x, y, \tau) \hat{\psi}(x, y, \tau) \hat{\psi}^{\dagger}(x, y, 0) \hat{\psi}(x, y, 0) \rangle, \quad (11)$$

$\chi_{\text{charge}}$  displays clear peaks at the edge for the FM phase and all the way to the critical point as shown in Fig. 3(a), reflecting the compressible nature of the gapless helical edge, as expected. More remarkably, we have found a large local charge compressibility of the bulk of the CAF state, as shown in Fig. 3. We have verified that this large susceptibility is also present in the uniform case in the absence of the edge potential. As a cross check, we consider a periodic system ( $\Delta = 0$ ) in presence of a finite pinning potential  $H_{\text{Pin}} = h_P \int d^2 \mathbf{x} \hat{\psi}^{\dagger}(x, y) \tau^z \otimes \sigma^z \hat{\psi}(x, y)$ . We have found that  $\chi_{\text{charge}}$  is suppressed, as shown in Fig. 3(b), demonstrating that this enhanced local charge susceptibility arises from the spontaneous symmetry breaking of CAF and its associated Goldstone mode.

*Discussion.* We have investigated via a large scale sign-problem-free QMC technique a topological phase transition realized in the quantum Hall regime of graphene at neutrality. This is a transition from a spin polarized (FM) state with counter-propagating helical edge modes, protected by the spin conservation and a non-trivial bulk spin Chern number, into a canted-antiferromagnetic that spontaneously breaks spin conservation, accompanied by a concomitant gapping of the helical edge modes. We have computed the electron local density of states, which is a quantity amenable to be probed in scanning tunneling microscopy. We have seen that the quasiparticle dispersions of the FM state display

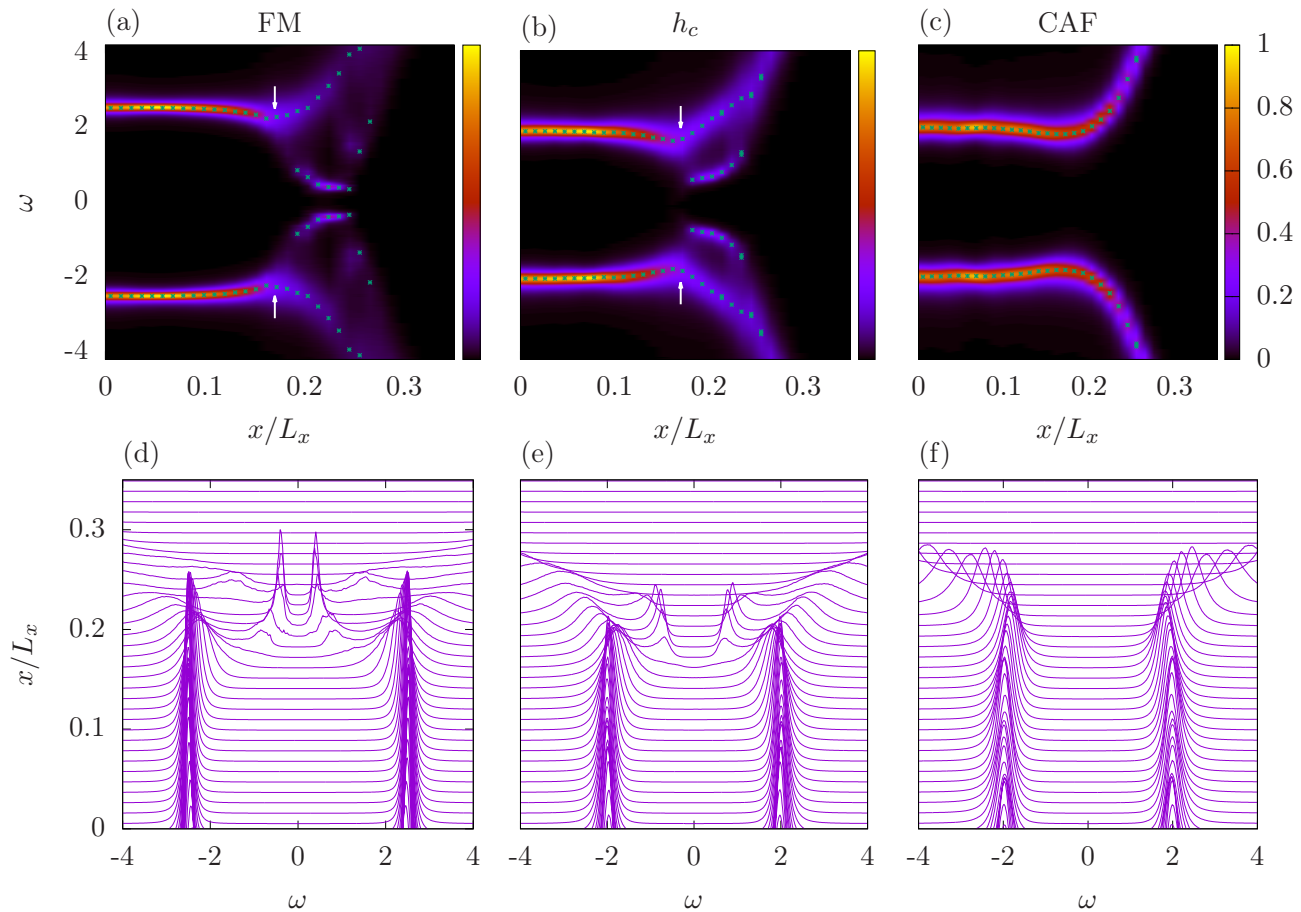


FIG. 2. Real space density of states  $A_\psi(x, \omega)$  for  $h = 1.2$  ((a),(d)),  $2/\pi$  ((b),(e)) and  $0.2$  ((c),(f)). Green dots are local maximums of  $A_\psi(x, \omega)$  as a function of  $\omega$ . White arrows are guides to the eye for the kinks of spectrum.

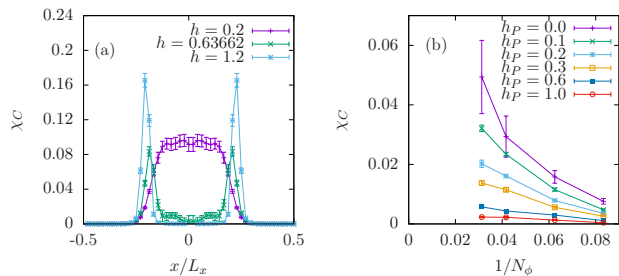


FIG. 3. (a). Real space dependence of  $\chi_C(x)$  at  $h = 0.2, 0.63662$  and  $1.2$  for  $N_\phi = 48$ . We took the vacuum potential  $\Delta = 6$ . (b).  $N_\phi$  dependence of spatially averaged  $\chi_C$  at  $h = 0.2$ , for  $\Delta = 0$ . We took  $\beta = N_\phi$  and the trotter step as  $\Delta\tau = 8/N_\phi$ .

non-monotonicity and kink-like features that are not present in the simplified mean field treatment of Ref. [27], but are reminiscent of those found in more systematic Hartree-Fock models of the edge [29]. We have also studied the local charge susceptibility and demonstrated that the edge of the spin polarized state remains substantially

compressible all the way to the critical point, beyond which a full charge gap appears in both the edge and the bulk. Interestingly, we have found that the CAF state has a large local bulk charge susceptibility that can be suppressed by pinning the Goldstone mode. These charge susceptibilities are amenable to be probed by local compressibility measurements.

ZW would like to thank Fakhre F. Assaad and Peng Rao for helpful discussions. The authors gratefully acknowledge the Gauss Centre for Supercomputing e.V. ([www.gauss-centre.eu](http://www.gauss-centre.eu)) for funding this project by providing computing time on the GCS Supercomputer SUPERMUC-NG at Leibniz Supercomputing Centre ([www.lrz.de](http://www.lrz.de)). DJL acknowledges support by the DFG through SFB 1143 (project-id 247310070) and the cluster of excellence ML4Q (EXC2004, project-id 390534769).

[1] B. E. Feldman, B. Krauss, J. H. Smet, and A. Yacoby, *Science* **337**, 1196 (2012),

- <https://www.science.org/doi/pdf/10.1126/science.1224784>.
- [2] B. E. Feldman, A. J. Levin, B. Krauss, D. A. Abanin, B. I. Halperin, J. H. Smet, and A. Yacoby, *Phys. Rev. Lett.* **111**, 076802 (2013).
- [3] F. Yang, A. A. Zibrov, R. Bai, T. Taniguchi, K. Watanabe, M. P. Zaletel, and A. F. Young, *Phys. Rev. Lett.* **126**, 156802 (2021).
- [4] A. A. Zibrov, E. M. Spanton, H. Zhou, C. Kometter, T. Taniguchi, K. Watanabe, and A. F. Young, *Nature Physics* **14**, 930 (2018).
- [5] P. Stepanov, S. Che, D. Shcherbakov, J. Yang, R. Chen, K. Thilakar, G. Voigt, M. W. Bockrath, D. Smirnov, K. Watanabe, T. Taniguchi, R. K. Lake, Y. Barlas, A. H. MacDonald, and C. N. Lau, *Nature Physics* **14**, 907 (2018).
- [6] A. T. Pierce, Y. Xie, S. H. Lee, P. R. Forrester, D. S. Wei, K. Watanabe, T. Taniguchi, B. I. Halperin, and A. Yacoby, *Nature Physics* **18**, 37 (2022).
- [7] D. S. Wei, T. van der Sar, S. H. Lee, K. Watanabe, T. Taniguchi, B. I. Halperin, and A. Yacoby, *Science* **362**, 229 (2018), <https://www.science.org/doi/pdf/10.1126/science.aar4061>.
- [8] A. Assouline, M. Jo, P. Brasseur, K. Watanabe, T. Taniguchi, T. Jolicoeur, D. C. Glatli, N. Kumada, P. Roche, F. D. Parmentier, and P. Roulleau, *Nature Physics* **17**, 1369 (2021).
- [9] H. Fu, K. Huang, K. Watanabe, T. Taniguchi, and J. Zhu, *Phys. Rev. X* **11**, 021012 (2021).
- [10] H. Zhou, C. Huang, N. Wei, T. Taniguchi, K. Watanabe, M. P. Zaletel, Z. Papić, A. H. MacDonald, and A. F. Young, “Strong-magnetic-field magnon transport in monolayer graphene,” (2021), arXiv:2102.01061 [cond-mat.mes-hall].
- [11] D. S. Wei, T. van der Sar, J. D. Sanchez-Yamagishi, K. Watanabe, T. Taniguchi, P. Jarillo-Herrero, B. I. Halperin, and A. Yacoby, *Science Advances* **3**, e1700600 (2017), <https://www.science.org/doi/pdf/10.1126/sciadv.1700600>.
- [12] S. Kim, J. Schwenk, D. Walkup, Y. Zeng, F. Ghahari, S. T. Le, M. R. Slot, J. Berwanger, S. R. Blanken-ship, K. Watanabe, T. Taniguchi, F. J. Giessibl, N. B. Zhitenev, C. R. Dean, and J. A. Stroscio, *Nature Communications* **12**, 2852 (2021).
- [13] A. K. Paul, M. R. Sahu, K. Watanabe, T. Taniguchi, J. Jain, G. Murthy, and A. Das, arXiv preprint arXiv:2205.00710 (2022).
- [14] Y. Zhang, Z. Jiang, J. P. Small, M. S. Purewal, Y.-W. Tan, M. Fazlollahi, J. D. Chudow, J. A. Jaszczak, H. L. Stormer, and P. Kim, *Phys. Rev. Lett.* **96**, 136806 (2006).
- [15] Z. Jiang, Y. Zhang, H. L. Stormer, and P. Kim, *Phys. Rev. Lett.* **99**, 106802 (2007).
- [16] A. F. Young, C. R. Dean, L. Wang, H. Ren, P. Cadden-Zimansky, K. Watanabe, T. Taniguchi, J. Hone, K. L. Shepard, and P. Kim, *Nature Physics* **8**, 550 (2012).
- [17] P. Maher, C. R. Dean, A. F. Young, T. Taniguchi, K. Watanabe, K. L. Shepard, J. Hone, and P. Kim, *Nature Physics* **9**, 154 (2013).
- [18] A. F. Young, J. D. Sanchez-Yamagishi, B. Hunt, S. H. Choi, K. Watanabe, T. Taniguchi, R. C. Ashoori, and P. Jarillo-Herrero, *Nature* **505**, 528 (2014).
- [19] L. Veyrat, C. Déprez, A. Coissard, X. Li, F. Gay, K. Watanabe, T. Taniguchi, Z. Han, B. A. Piot, H. Sellier, and B. Sacépé, *Science* **367**, 781 (2020), <https://www.science.org/doi/pdf/10.1126/science.aax8201>.
- [20] I. Sodemann and A. H. MacDonald, *Phys. Rev. Lett.* **112**, 126804 (2014).
- [21] D. A. Abanin, B. E. Feldman, A. Yacoby, and B. I. Halperin, *Phys. Rev. B* **88**, 115407 (2013).
- [22] S.-Y. Li, Y. Zhang, L.-J. Yin, and L. He, *Phys. Rev. B* **100**, 085437 (2019).
- [23] X. Liu, G. Farahi, C.-L. Chiu, Z. Papić, K. Watanabe, T. Taniguchi, M. P. Zaletel, and A. Yazdani, *Science* **375**, 321 (2022), <https://www.science.org/doi/pdf/10.1126/science.abm3770>.
- [24] A. Coissard, D. Wander, H. Vignaud, A. G. Grushin, C. Repellin, K. Watanabe, T. Taniguchi, F. Gay, C. Winkelmann, H. Courtois, H. Sellier, and B. Sacépé, “Imaging tunable quantum hall broken-symmetry orders in charge-neutral graphene,” (2021).
- [25] D. A. Abanin, P. A. Lee, and L. S. Levitov, *Phys. Rev. Lett.* **96**, 176803 (2006).
- [26] E. Shimshoni, H. A. Fertig, and G. V. Pai, *Phys. Rev. Lett.* **102**, 206408 (2009).
- [27] M. Kharitonov, *Phys. Rev. B* **86**, 075450 (2012).
- [28] G. Murthy, E. Shimshoni, and H. A. Fertig, *Phys. Rev. B* **90**, 241410 (2014).
- [29] A. Knothe and T. Jolicoeur, *Phys. Rev. B* **92**, 165110 (2015).
- [30] G. Murthy, E. Shimshoni, and H. A. Fertig, *Phys. Rev. B* **93**, 045105 (2016).
- [31] H. A. Fertig and L. Brey, *Phys. Rev. Lett.* **97**, 116805 (2006).
- [32] M. Kharitonov, *Phys. Rev. B* **85**, 155439 (2012).
- [33] See however Ref. [50] for an interesting recent study beyond this model.
- [34] D. N. Sheng, Z. Y. Weng, L. Sheng, and F. D. M. Haldane, *Phys. Rev. Lett.* **97**, 036808 (2006).
- [35] C. L. Kane and E. J. Mele, *Phys. Rev. Lett.* **95**, 226801 (2005).
- [36] C. L. Kane and E. J. Mele, *Phys. Rev. Lett.* **95**, 146802 (2005).
- [37] M. Ippoliti, R. S. K. Mong, F. F. Assaad, and M. P. Zaletel, *Phys. Rev. B* **98**, 235108 (2018).
- [38] Z. Wang, M. P. Zaletel, R. S. K. Mong, and F. F. Assaad, “Phases of the (2+1) dimensional so(5) non-linear sigma model with topological term,” (2020), arXiv:2003.08368 [cond-mat.str-el].
- [39] R. Blankenbecler, D. J. Scalapino, and R. L. Sugar, *Phys. Rev. D* **24**, 2278 (1981).
- [40] S. White, D. Scalapino, R. Sugar, E. Loh, J. Gubernatis, and R. Scalettar, *Phys. Rev. B* **40**, 506 (1989).
- [41] F. Assaad and H. Evertz, in *Computational Many-Particle Physics*, Lecture Notes in Physics, Vol. 739, edited by H. Fehske, R. Schneider, and A. Weiße (Springer, Berlin Heidelberg, 2008) pp. 277–356.
- [42] A. Collaboration, F. F. Assaad, M. Berx, F. Goth, A. Götz, J. S. Hofmann, E. Huffman, Z. Liu, F. P. Toldin, J. S. E. Portela, and J. Schwab, (2021), arXiv:2012.11914 [cond-mat.str-el].
- [43] A. F. Young, J. D. Sanchez-Yamagishi, B. Hunt, S. H. Choi, K. Watanabe, T. Taniguchi, R. C. Ashoori, and P. Jarillo-Herrero, *Nature* **505** (2014), 10.1038/nature12800.
- [44] B. E. Feldman, B. Krauss, J. H. Smet, and A. Yacoby, *Science* **337**, 1196 (2012), <https://www.science.org/doi/pdf/10.1126/science.1224784>.
- [45] B. E. Feldman, A. J. Levin, B. Krauss, D. A. Abanin,

- B. I. Halperin, J. H. Smet, and A. Yacoby, *Phys. Rev. Lett.* **111**, 076802 (2013).
- [46] A. A. Zibrov, E. M. Spanton, H. Zhou, C. Kometter, T. Taniguchi, K. Watanabe, and A. F. Young, *Nature Physics* **14** (2018), 10.1038/s41567-018-0190-0.
- [47] S. S. Hegde and I. S. Villadiego, “Theory of competing charge density wave, kekule and antiferromagnetic ordered fractional quantum hall states in graphene aligned with boron nitride,” (2022), arXiv:2202.01796 [cond-mat.mes-hall].
- [48] I. Sodemann and M. M. Fogler, *Phys. Rev. B* **86**, 115408 (2012).
- [49] K. S. D. Beach, P. A. Lee, and P. Monthoux, *Phys. Rev. Lett.* **92**, 026401 (2004).
- [50] A. Das, R. K. Kaul, and G. Murthy, *Phys. Rev. Lett.* **128**, 106803 (2022).

## SUPPLEMENTAL MATERIAL

### A. Quantum Monte Carlo implementation and examination of bulk phase transition

We summarize the QMC implementation in this section. The spatial coordinate  $\mathbf{x}$  lives on a torus of size  $L_x \times L_y$ . We choose  $L_x = 4L_y$  for the calculation. The fermion annihilation operators are projected onto the ZLL:  $\hat{\psi}_a(\mathbf{x}) = \sum_{n_k=1}^{N_\phi} \phi_{n_k}(\mathbf{x}) \hat{c}_{a,n_k}$ . The index  $a$  runs over 1...4 corresponding to the four flavors constructed via physical spin and graphene sublattice. The wave functions for the ZLL,  $\phi_{n_k}(\mathbf{x})$ , are defined in the Landau gauge with translational invariance along  $y$  direction.  $y$  direction momentum  $k_y$  is a good quantum number ( $k_y = \frac{2\pi n_k}{L_y}$ ). To implement QMC, we rewrite the various generalized pseudo-spin density interactions in momentum space, as follows:

$$\begin{aligned} \hat{\psi}^\dagger(\mathbf{x}) O^i \hat{\psi}(\mathbf{x}) &= \frac{1}{V} \sum_{\mathbf{q}} e^{-i\mathbf{q}\cdot\mathbf{x}} \hat{n}^i(\mathbf{q}) \\ \hat{n}^i_{\mathbf{q}} &= \sum_k f(\mathbf{q}) e^{\frac{i}{2}(2k-q_y)l_B^2 q_x} [\hat{c}_k^\dagger O^i \hat{c}_{k-q_y - [\frac{k-q_y}{2\pi N_\phi/L_y]} \frac{2\pi N_\phi}{L_y}} \\ &\quad - 2\delta_{q_y,0} \delta_{i,0}] \quad f(\mathbf{q}) = e^{-\frac{1}{4}l_B^2 |\mathbf{q}|^2} \end{aligned} \quad (12)$$

where  $O^i$  denote  $4 \times 4$  matrices in valley space  $\tau^z, \tau^x, \tau^y$  and  $\mathbb{1}$  for  $i = 1, 2, 3, 0$ , respectively. A complex Hubbard-Stratonovich transformation is performed to decouple the interaction operators for each momentum  $\mathbf{q}$ . The absence of the sign problem is guaranteed by two anti-unitary particle-hole symmetries  $\tau^z \sigma^x P$  and  $\tau^z \sigma^y P$  ( $P \alpha \hat{c}_k P^{-1} \equiv \bar{\alpha} \hat{c}_k^\dagger$ ) that anti-commute with each other. As shown in Ref. [38], difficulties of this simulation arise from the compactness of the projected density operators in single particle Hilbert space as well as from the non-local commutation relation between them. Hence the systematic Trotter error scales maximally as  $\Delta\tau^2 N_\phi^2$ , [38] and the CPU time scales as  $\beta N_\phi^5$ . Regularization in momentum space is based on a truncation from the exponential energy factor in density operator such that terms with  $f(\mathbf{q}) < 10^{-2}$  is omitted. On the other hand, the simulation is less efficient than the one in Ref. [38] due to the breaking of  $SU(2)$  spin symmetry by a finite Zeeman coupling.

Switching on a finite in-plane magnetic field, we reproduce the CAF-FM bulk phase diagram as a function of  $h$ . To detect the  $U(1)$  symmetry breaking of the CAF state, we compute the order parameter correlation function

$$S(\mathbf{q})_{\text{CAF}} = \frac{1}{N_\phi} \langle \hat{m}_{\mathbf{q}} \hat{m}_{-\mathbf{q}} \rangle. \quad (13)$$

Here  $\hat{m}(\mathbf{q})$  is the operator from Eq. 12 corresponding to  $\tau^z \sigma^x$  (Neel order parameter). For an ordering wave

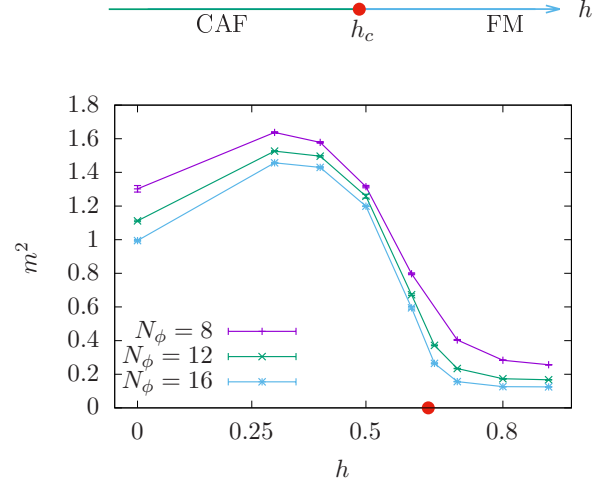


FIG. 4. (a) Ground state phase diagram of the bulk. (b) CAF squared magnetization  $m_{\text{CAF}}$  as a function of Zeeman coupling  $h$ .

vector  $\mathbf{Q} = 0$ , the local moment (magnetization) reads

$$m_{\text{CAF}} = \sqrt{\frac{1}{N_\phi} S(\mathbf{Q})} \quad (14)$$

As shown in Fig. 4, magnetic ordering develops as long as  $h < h_c$ , with a value of  $h_c$  consistent with mean field theory and previous studies [32]. Here we took  $\beta = N_\phi$  such that the simulation is converged to the ground state for each system size, and  $\Delta\tau = 2/N_\phi$ .

### B. Mean field calculation

In Hartree-Fork (HF) we use the following Slater-determinate state

$$|\Psi\rangle \equiv \prod_{n_k=1}^{N_\phi} \prod_{a=1}^2 \left( \sum_{b=1}^4 P_{ab} \hat{c}_{b,k}^\dagger \right) |0\rangle \quad (15)$$

as mean field wave function. Here the  $4 \times 4$  matrix  $P$  is defined as a projector:

$$P \equiv \frac{1}{2} (\mathbb{1}_4 + \sin \theta \tau^z \sigma^x + \cos \theta \sigma^z) \quad (16)$$

Hence  $\text{Tr} P = 2$  and  $\Psi$  is normalized.  $\theta = \frac{\pi}{2}$  implies an AF ordering without canting and  $\theta = 0$  implies a polarized FM state.

The  $g_z$  part of the interaction ( $-\frac{1}{2N_\phi} g_z \hat{n}_{-\mathbf{Q}}^i \hat{n}_{\mathbf{Q}}^i$ ) con-



tributes a mean field energy of

$$\begin{aligned}
E_Z &= \frac{1}{4\pi} g_z (\text{Tr}[P\tau_z]^2 - \text{Tr}[P\tau_z P\tau_z]) \sum_{\mathbf{q}} f(\mathbf{q}) f(-\mathbf{q}) \\
&= -\frac{1}{4\pi} g_z (1 + \cos^2 \theta + \sin^2 \theta) N_\phi \\
&= -\frac{g_z}{2\pi} N_\phi
\end{aligned} \tag{17}$$

where  $f(\mathbf{q}) \equiv \exp(-\frac{1}{4}|\mathbf{q}|^2 l_B^2)$  is the exponentially decaying form factor of the density operator.

The  $g_\perp$  part of the interaction contributes mean field energy of

$$\begin{aligned}
E_\perp &= \frac{1}{4\pi} 2g_\perp (\text{Tr}[P\tau_x]^2 - \text{Tr}[P\tau_x P\tau_x]) \sum_{\mathbf{q}} f(\mathbf{q}) f(-\mathbf{q}) \\
&= -\frac{1}{2\pi} g_\perp (1 + \cos^2 \theta - \sin^2 \theta) N_\phi \\
&= -\frac{g_\perp}{\pi} \cos^2 \theta N_\phi
\end{aligned} \tag{18}$$

On the other hand the  $SU(4)$  invariant Coulomb interaction  $g_0$  does not contribute to the mean field energy.

The ground state mean field energy, considering all the interactions as well as Zeeman coupling is then

$$\begin{aligned}
E_{MF}/N_\phi &= -\frac{g_z + 2g_\perp \cos^2 \theta}{2\pi} g_z - 2h \cos \theta \\
&= \frac{-g_z + 2|g_\perp| \cos^2 \theta}{2\pi} - 2h \cos \theta
\end{aligned} \tag{19}$$

Hence the minimal energy happens at  $\cos \theta = \frac{\pi h}{g_\perp}$ .

And the mean field Hamiltonian reads

$$\hat{H}_{MF} = \sum_{n_k=1}^{N_\phi} \hat{c}_k^\dagger h_{\text{int}} \hat{c}_k - h \sum_{n_k=1}^{N_\phi} \hat{c}_k^\dagger \sigma_z \hat{c}_k \tag{20}$$

where

$$\begin{aligned}
h_{\text{int}} &= \frac{1}{2\pi} \left[ \sum_{i=1}^3 g_i [T^i \text{Tr}(PT^i) - T^i PT^i] - \tilde{g}_0 P \right] \\
&= \frac{1}{4\pi} (-\tilde{g}_0 - g_z + 2g_\perp) \sin \theta \tau^z \sigma^x \\
&+ \frac{1}{4\pi} (-\tilde{g}_0 - g_z - 2g_\perp) \cos \theta \sigma^z \\
&= \frac{1}{4\pi} (-\tilde{g}_0 - g_z - 2|g_\perp|) \sin \theta \tau^z \sigma^x \\
&+ \frac{1}{4\pi} (-\tilde{g}_0 - g_z + 2|g_\perp|) \cos \theta \sigma^z
\end{aligned} \tag{21}$$

where mean field contribution from Coulomb interactions is

$$\tilde{g}_0 = \frac{e^2}{\epsilon l_B} \sum_{\mathbf{q}} \frac{f(\mathbf{q}) f(-\mathbf{q}) V_0(\mathbf{q})}{N_\phi} \tag{22}$$

The momentum dependent potential is the Fourier component of  $V(|\mathbf{x} - \mathbf{x}'|)$  in main text:

$$V_0(\mathbf{q}) = \frac{1}{|\mathbf{q}| l_B} (1 - e^{-|\mathbf{q}| l_B}) \tag{23}$$

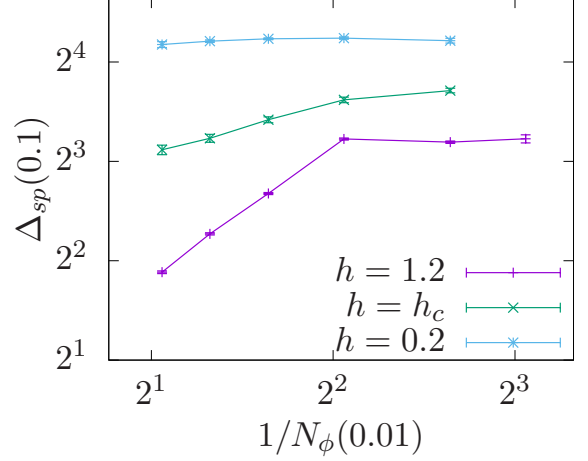


FIG. 5.  $1/N_\phi$  dependence of  $\Delta_{sp}$  in log-log scale.

Due to the anti-commutation relation between  $\sigma^z$  and  $\tau^z \sigma^x$ , the one particle excitation gap of Eq. 20 is

$$\begin{aligned}
\Delta_{sp} &= \left\{ \left[ \frac{1}{4\pi} (\tilde{g}_0 + g_z - 2|g_\perp|) \cos \theta + h \right]^2 \right. \\
&\quad \left. + \left[ \frac{1}{4\pi} (\tilde{g}_0 + g_z + 2|g_\perp|) \sin \theta \right]^2 \right\}^{1/2}
\end{aligned} \tag{24}$$

where the phase angle is given by  $\cos \theta = \pi h / g_\perp$ .

### C. Finite size dependence of single particle gap

In this section we show the finite size dependence of single particle excitation gap at the edge. We extrapolate the gap  $\Delta_{sp}$  asymptotically based on:

$$\sum_a \langle \hat{\psi}_a^\dagger(x, y, \tau) \hat{\psi}_a(x, y, 0) \rangle \propto e^{-\Delta_{sp}(x)\tau} \tag{25}$$

for large  $\tau$ . We take edge gap as  $\Delta_{sp} \equiv \min\{\Delta_{sp}(x)\}$ . Fig. 5 displays the system size dependence of  $\Delta_{sp}$  for three values of Zeeman coupling. A linear behavior on a doubly logarithmic scale indicates vanishing value of  $\Delta_{sp}$  in the thermodynamic limit for the case of  $h = 1.2$  and  $h_c = 2/\pi$ .

### D. Vanishing long range Coulomb interaction case

We claimed in the main text that the broadening of the quasi-particle peak at  $h_c$  is mainly induced by strong long range Coulomb interaction that which are  $SU(4)$  invariant. Here we show the LDOS in the absence of  $\hat{H}_{\text{Coul}}$ . As shown in Fig. 6, finite size gap along the edge vanishes and the spectral weight shows well defined quasi-particle behavior, which is close to the one from mean field analysis [27].



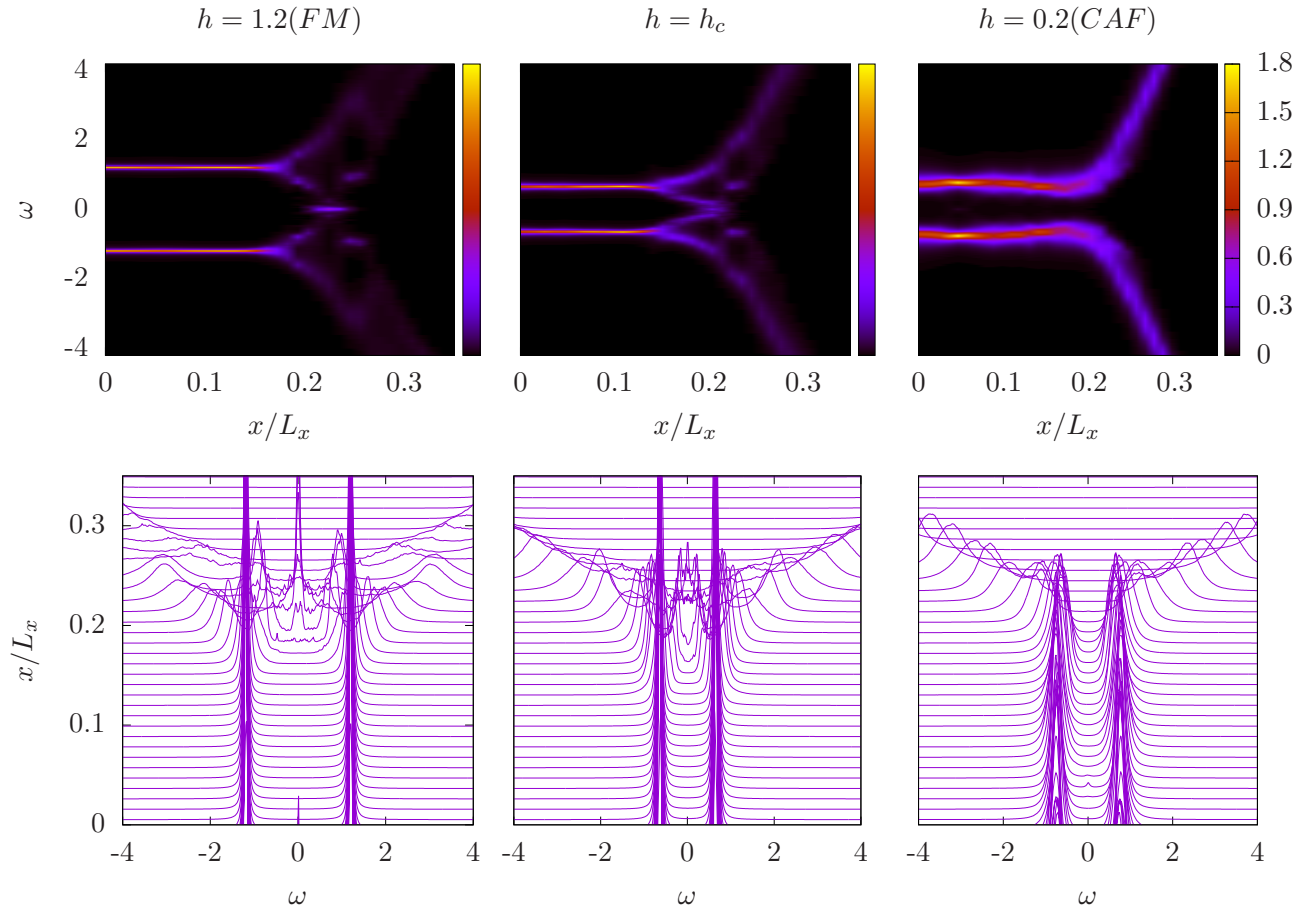


FIG. 6. Same as Fig. 2 in main text, for  $\hat{H}_{\text{Coul}} = 0$ .